materials

MDPI

Article

Synthesis and Characterization of Li_2MgGeO_4:Ho^{3+}

Nikola Bednarska-Adam [1,*], Marta Kuwik [1], Ewa Pietrasik [1], Wojciech A. Pisarski [1], Tomasz Goryczka [2], Bogusław Macalik [3] and Joanna Pisarska [1,*]

[1] Institute of Chemistry, University of Silesia, 9 Szkolna Street, 40-007 Katowice, Poland; marta.kuwik@us.edu.pl (M.K.); ewa.pietrasik@us.edu.pl (E.P.); wojciech.pisarski@us.edu.pl (W.A.P.)
[2] Institute of Materials Engineering, University of Silesia, 75 Pułku Piechoty 1A Street, 41-500 Chorzów, Poland; tomasz.goryczka@us.edu.pl
[3] Institute of Low Temperature and Structure Research, Polish Academy of Sciences, Okólna 2 Street, 50-422 Wrocław, Poland; b.macalik@int.pan.wroc.pl
* Correspondence: nikola.bednarska@us.edu.pl (N.B.-A.); joanna.pisarska@us.edu.pl (J.P.)

Abstract: In this work, the synthesis and characterization of Li_2MgGeO_4:Ho^{3+} ceramics were reported. The X-ray diffraction measurements revealed that the studied ceramics belong to the monoclinic Li_2MgGeO_4. Luminescence properties were analyzed in the visible spectral range. Green and red emission bands correspondent to the $^5F_4$,$^5S_2 \rightarrow {}^5I_8$ and $^5F_5 \rightarrow {}^5I_8$ transitions of Ho^{3+} were observed, and their intensities were significantly dependent on activator concentration. Luminescence spectra were also measured under direct excitation of holmium ions or ceramic matrix. Holmium ions were inserted in crystal lattice Li_2MgGeO_4, giving broad blue emission and characteristic 4f-4f luminescent transitions of rare earths under the selective excitation of the ceramic matrix. The presence of the energy transfer process between the host lattice and Ho^{3+} ions was suggested.

Keywords: Li_2MgGeO_4; Ho^{3+} ions; structure; luminescence

Citation: Bednarska-Adam, N.; Kuwik, M.; Pietrasik, E.; Pisarski, W.A.; Goryczka, T.; Macalik, B.; Pisarska, J. Synthesis and Characterization of Li_2MgGeO_4:Ho^{3+}. *Materials* **2022**, *15*, 5263. https://doi.org/10.3390/ma15155263

Academic Editor: Efrat Lifshitz

Received: 28 June 2022
Accepted: 27 July 2022
Published: 29 July 2022

1. Introduction

Holmium-doped materials are really interesting optical systems due to several 4f-4f electronic transitions operating in the visible and near-IR spectral ranges [1–4]. The energy level diagram of Ho^{3+} ions favors various radiative and non-radiative pathways dependent on the activator concentration, excitation wavelengths, host matrices, and their phonon energies. Trivalent holmium ions were introduced to numerous inorganic glasses [5–9], ceramics [10–12], and other nanoparticles synthesized using the sol–gel method [13]. Special attention has been paid to Ho^{3+}-doped ceramic phosphors with superior luminescence properties. Ho^{3+}-doped (K,Na)NbO_3-based multifunctional ceramics present excellent optical temperature-sensing performance [14]. Such systems possess an optical temperature sensitivity higher than other rare-earth-doped ceramics or glasses, suggesting their attractive applications, especially in temperature-sensing devices. The same situation was also observed for similar Ho^{3+}-doped ceramic compounds [15–18]. These aspects were also reported in the excellent review that was published recently [19]. Holmium-doped $Y_2Zr_2O_7$ ceramics [20] were proposed as a new type of laser materials emitting visible light. The experimental results demonstrate that $Y_2Zr_2O_7$:Ho^{3+} ceramics are able to generate efficient down- and upconversion luminescence. Further studies revealed that Y_2O_3-MgO:Ho^{3+} ceramics are novel IR-transparent nanocomposite ceramics [21] that can be applied to high-power eye-safe near-infrared lasers operating at about 2000 nm.

In this work, we show preliminary results for holmium-doped Li_2MgGeO_4:Ho^{3+} germanate ceramics. In particular, their visible emission properties under different excitation wavelengths were examined in detail. These germanate ceramic systems are less documented in the literature. The previously published works were mainly concentrated on luminescence investigations of Li_2MgGeO_4:Mn^{2+}. Germanate ceramic Li_2MgGeO_4:Mn^{2+} was

proposed as a green long-persistent phosphor [22]. Trap-controlled reproducible mechanoluminescent (ML) $Li_2MgGeO_4:Mn^{2+}$ materials were also developed, and their short-term non-decaying ML behavior was reported [23]. Further investigations offering a constructive prospect for developing novel functional mechanoluminescent $Li_2MgGeO_4:xMn^{2+}$ phosphors by defect control are also presented and discussed [24]. Optical properties of rare earths, especially Ho^{3+} ions in Li_2MgGeO_4 ceramics, have not yet been reported, to the best of our knowledge. Therefore, the synthesis and characterization of $Li_2MgGeO_4:Ho^{3+}$ are exhibited here.

2. Experimental Methods

Germanate ceramics were characterized by a SETARAM Labsys thermal analyzer (SETERAM Instrumentation, Caluire, France) using the DSC method. The DSC curve was acquired in the range from room temperature to 1100 °C at the standard rate of 10 °C/min. The X-ray diffraction patterns were measured using an X'Pert-Pro diffractometer (PANalytical, Eindhoven, The Netherlands). The microstructure of germanate ceramics was observed using a JSM6480 scanning electron microscope (Jeol Ltd., Tokyo, Japan) as well as a JSM-7100F TTL LV (Jeol Ltd., Tokyo, Japan). The UV-VIS diffuse-reflectance spectra were collected using a Cary 5000 UV–VIS–NIR spectrophotometer, (Agilent Technology, Santa Clara, CA, USA). Excitation and luminescence measurements were carried out on a Photon Technology International (PTI) Quanta-Master 40 (QM40) UV/VIS Steady State Spectrofluorometer coupled with a tunable pulsed optical parametric oscillator (OPO) pumped by a third harmonic of a Nd:YAG laser (Opotek Opolette 355 LD, OPOTEK, Carlsband, CA, USA). The laser system included a double 200 mm monochromator, a xenon lamp as a light source, and a multimode UVVIS PMT (R928) (PTI Model 914, Horiba Instruments, New York, NY, USA) detector. The spectral resolution was equal to 0.5 nm. The Commission Internationale de l'Eclairage (CIE) chromaticity coordinates (x, y) and chromaticity diagram for Li_2MgGeO_4 ceramics doped with Ho^{3+} ions were calculated from the emission spectra and plotted using *Color Calculator* software (*Osram* Sylvania, Inc., Wilmington, MA, USA). Decay curves were recorded by a PTI ASOC-10 [USB-2500] oscilloscope (Horiba Instruments, New York, NY, USA) with an accuracy of ±0.5 μs. All experiments were carried out at room temperature.

3. Results and Discussion

3.1. Synthesis

Holmium-doped germanate ceramics with the following chemical compositions $Li_2Mg_{(100-x)}GeO_4:xHo^{3+}$ in molar % (where x = 0, 0.5, 2.5, and 5) were prepared by the solid-state reaction method using precursor powders of high purity (Sigma-Aldrich Chemical Co., St. Louis, MO, USA). The initial reagents Li_2CO_3 (99.997%), MgO (99.99%), GeO_2 (99.99%), and optical active dopant Ho_2O_3 (99.999%) were weighed in stoichiometric amounts and mixed together homogeneously in an agate mortar for 1 h with ethanol (POCH Basic 96% pure) as a medium.

After the samples were grounded, the mixtures were calcinated in the muffle furnace (FCF 5 5SHP produced by Czylok, Jastrzębie-Zdrój, Poland) in a non-covered platinum crucible at 1100 °C for 6 h in the ambient air to achieve decarbonization. According to the results for similar Li_2SrGeO_4 phosphors obtained by Huang and Li [25], the following reaction takes place during calcination:

$$Li_2CO_3 + SrCO_3 + GeO_2 \rightarrow Li^+ + Sr^{2+} + Ge^{4+} + O^{2-} \rightarrow Li_2SrGeO_4$$

Thus, it can be assumed that for the synthesized $Li_2MgGeO_4:Ho^{3+}$ ceramics, referred to here as LMG-Ho^{3+}, the following reaction occurs:

$$Li_2CO_3 + MgO + GeO_2 + Ho_2O_3 \rightarrow Li^+ + Mg^{2+} + Ge^{4+} + O^{2-} + Ho^{3+} \rightarrow Li_2MgGeO_4:Ho^{3+}$$

The calcination process consisted of two steps. The temperature was increased to T = 800 °C in 30 min, then the furnace reached 1100 °C in 10 min. The samples were kept at this temperature for 5 h and 20 min.

In the next step, the granulated powders were divided into smaller batches and then mixed with an organic binder for 0.5 h. Among possible binders, polyvinyl alcohol (PVA) can be successfully used to receive germanate ceramic pellets. In general, PVA was often used as a binder [26–29]. The mixtures were uniaxially pressed into pellets of 10 mm diameter under 375 MPa. The prepared pellets were gradually heated to remove the PVA binder at 550 °C. The temperature was raised by 3 °C/min until the appropriate temperature was achieved. The samples were annealed for 2 h under ambient air conditions and naturally cooled to room temperature.

Lastly, the ceramic samples were sintered in a high-temperature furnace (FCF 4/170M produced by Czylok, Jastrzębie-Zdrój, Poland) at 1200 °C for 5 h. The thermal and structural results for olivine-type germanates presented previously and discussed by Koseva et al. [30] indicate that the annealing temperature of 1373 K (1100 °C) is optimal for obtaining well-crystallized phase-pure samples. It is worth noting that germanium dioxide has a low melting point at 1115 °C; therefore, the germanate olivines have low sintering temperatures [31]. In our synthesis procedure, the free sintering process consisted of several steps. First, the temperature was increased up to 800 °C for 1 h, and the samples were sintered without increasing the temperature for 15 min. Next, the furnace was heated to 1200 °C at a rate of 9 °C/min. The samples were sintered at the set temperature for 3 h. After this time, the resulting ceramics were cooled down to room temperature in a closed furnace.

3.2. Characterization

Figure 1 presents a representative DSC curve (a) and X-ray diffraction patterns (b) recorded for the studied LMG-Ho^{3+} ceramic system.

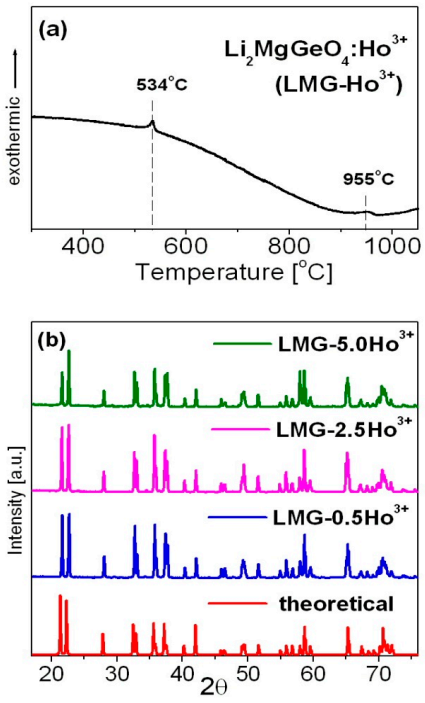

Figure 1. Representative DSC curve (**a**) and X-ray diffraction patterns (**b**) of LMG-Ho^{3+}.

Li_2MgGeO_4:Ho^{3+} germanate ceramics (LMG-Ho^{3+}) show two phase transitions [30]. The low-temperature phase transition near T = 534 °C is related to insignificant changes in the monoclinic symmetry. The high-temperature phase transition at about 955 °C is

assigned to the transition from monoclinic to orthorhombic symmetry. The X-ray diffraction analysis confirmed that the studied LMG-Ho^{3+} ceramic systems crystallize in a monoclinic crystal lattice. The narrow diffraction lines are in a good agreement with the theoretical pattern belonging to the monoclinic Li_2ZnGeO_4 (ICDD PDF-4 database—card no 04-015-4929), which is isostructural to Li_2MgGeO_4 [32]. The schematic crystal structure of Li_2ZnGeO_4 belonging to the same monoclinic crystal system with $P2_1/n$ space group as Li_2MgGeO_4 was presented by Lin et al. [33].

The introduction of Ho^{3+} playing the role of active doping ions to the host matrix Li_2MgGeO_4 do not cause any significant changes in the crystal structure. Independent of the Ho^{3+} concentration (0.5, 2.5, and 5 mol%), the XRD patterns without additional diffraction peaks due to impurities are almost consistent with pure Li_2MgGeO_4 monoclinic phase. This suggests that trivalent holmium ions are well-entered into the Li_2MgGeO_4 crystalline lattice. Furthermore, the Mg^{2+} ions are substituted by Ho^{3+} ions similar to Li_2AGeO_4 compounds, where the atomic positions of A^{2+} ions may be occupied by trivalent rare earth ions such as Ce^{3+}, Tb^{3+}, or Dy^{3+} [25]. The introduction of rare earth ions to the Li_2MgGeO_4 host matrix due to the substitution of a divalent cation (Mg^{2+}) by a trivalent ion (Ho^{3+}) can result in charge imbalance. It is well-known that charge compensation can be achieved by creating defects in the crystal lattice. The presence of defects in the ceramic host leads to the weakness of luminescent properties. However, the incorporation of alkali ions (Li^+ or Na^+) might compensate for the charge imbalance, reduce the lattice distortion, and enhance luminescence intensity without creating impurities in the host structure [34–38]. It should be also noted that agglomerates are present in the studied germanate ceramics. The diameter of agglomerates is changed from several dozen micrometers to even 150 µm. Most agglomerates have a diameter of around 40 µm. For the LMG-Ho^{3+} system, the grain sizes do not exceed 10 µm, which was verified using scanning electron microscopy (SEM). SEM images of the LMG-Ho^{3+} ceramic host are shown in Figure 2.

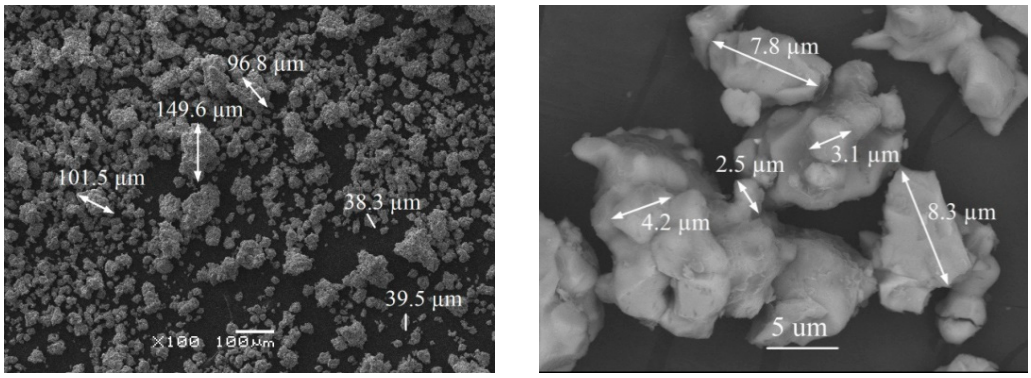

Figure 2. SEM images of LMG-Ho^{3+}.

Figure 3 presents the UV-VIS diffuse-reflectance spectra for LMG-Ho^{3+} ceramics with different concentrations of holmium ions (0.5, 2.5, and 5 mol%) that were registered at room temperature in the 225–800 nm spectral region. Several narrow absorption peaks corresponding to intra-configurational 4f-4f electronic transitions from ground state $^5I_8$ to higher-lying excited states of trivalent holmium are quite well observed. The registered absorption peaks are centered at about ~360 nm, ~415 nm, ~450 nm, ~535 nm, and ~635 nm and originated from the $^5I_8 \rightarrow {}^3H_{5,6}$; $^5I8 \rightarrow {}^3G_{4,5}$; $^5I_8 \rightarrow {}^5G_6, {}^5F_2, {}^3K_8$; $^5I_8 \rightarrow {}^5F_3$; $^5I_8 \rightarrow {}^5S_2, {}^5F_4$; and $^5I_8 \rightarrow {}^3F_5$ transitions, respectively [39]. The strongest absorption, located at 450 nm, is attributed to the $^5I_8 \rightarrow {}^2G_6, {}^5F_2, {}^3K_8$ transition of Ho^{3+} ions. The obtained results clearly show that with increasing optically active dopants the intensity of absorption peaks also increases, keeping the same intensity ratios between the recorded peaks.

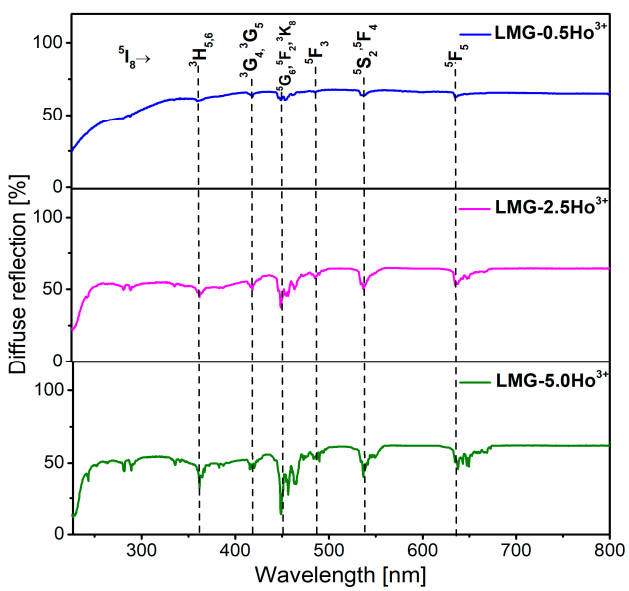

Figure 3. Reflectance spectra of LMG-0.5Ho^{3+}, LMG-2.5Ho^{3+}, and LMG-5.0Ho^{3+}.

The crucial aspect of analyzing the optical properties of transparent glass-ceramics, ceramics, and various phosphors is the characterization of the luminescence, which results from the 4f-4f electronic transitions of rare earth ions [40–47]. It is worth noting that studies of ceramic samples containing trivalent holmium ions are focused on characterizing the efficient green visible emission [6,18,48]. In general, as a result of the excitation of Ho^{3+} ions, the energy is transferred via non-radiative decay from higher-lying excited levels such as $^3H_5$, $^3H_6$, $^5G_4$, $^5G_5$, $^5G_8$, $^5F_2$, and $^5F_3$ to levels $^5F_4$, $^5S_2$, and $^5F_5$ of trivalent holmium ions. Afterward, the excitation energy is transferred to the ground state and causes emitting radiation due to characteristic transitions of Ho^{3+} ions. The emission spectra in the visible range, measured for the LMG-Ho^{3+} ceramic samples under the direct excitation of Ho^{3+} ions (λ_{exc} = 453 nm), consist of two well-separated bands (Figure 4).

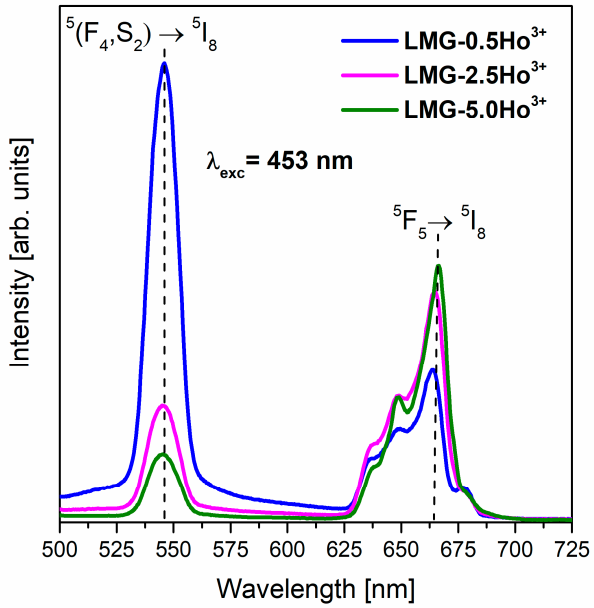

Figure 4. Luminescence spectra for LMG-Ho^{3+} ceramics with different contents of holmium ions.

Independent of the concentration of holmium ions in LMG ceramics, the emission bands located at 546 nm and 666 nm, corresponding to electronic transitions originating

from the $^5F_4$, $^5S_2$, and $^5F_5$ states to the ground state, $^5I_8$, were recorded, respectively. Both the band originating from the $^5F_4$,$^5S_2 \rightarrow ^5I_8$ transitions and the band associated with the $^5F_5 \rightarrow ^5I_8$ transition of Ho^{3+} ions are characterized by considerable emission intensity.

Our investigations clearly indicate that the relative integrated emission intensities due to the $^5F_4$,$^5S_2 \rightarrow ^5I_8$ (green) and $^5F_5 \rightarrow ^5I_8$ (red) transitions of Ho^{3+} ions in Li_2MgGeO_4 ceramics depend critically on activator concentration. The emission intensity of the green transition decreases, whereas the emission intensity of red transition is enhanced, with increasing Ho^{3+} ion concentrations. The observed intensities of green (546 nm) and red (666 nm) emissions for our ceramic samples are opposite in comparison to the $CaLa_4$-xSi_3O_{13}:Ho^{3+} phosphors reported by Singh et al. [49]. In this study, the $CaLa_4$-xSi_3O_{13} ceramics doped with holmium ions exhibited an intense green emission at 546 nm attributed to the $^5F_4$,$^5S_2 \rightarrow ^5I_8$ transitions, whereas the red emission from the $^5F_5 \rightarrow ^5I_8$ transition was significantly weaker. Moreover, Li et al. [50] registered dominant green emission under the direct excitation of Ho^{3+} ions in potassium sodium niobate-based ceramics. However, the emission intensity of the band corresponding to the $^5F_4$,$^5S_2 \rightarrow ^5I_8$ transitions decreased with increasing contents of optical active dopants (Ho^{3+}) in ceramic compositions. This phenomenon is attributed to the so-called the concentration luminescence quenching effect, which was also observed for holmium-doped $LiPbB_5O_9$ [51]. The results obtained for $LiPbB_5O_9$:Ho^{3+} indicated that the intensity of visible emission was increased for samples with low contents of Ho^{3+} (from 0.04 mol% to 0.08 mol%) and then decreased with further increases in the holmium ion concentration. Consequently, once the content of optical active dopants exceeds a critical value, the mechanism of concentration quenching is triggered [51]. The origin of this phenomenon is due to non-radiative energy transfer interactions between emitting activator ions. Energy transfer between them is more effective at high concentrations because the average distance between the activator ions is shorter, and the energy transfer probability is higher. Thus, the coupled excited states $^5F_4$ and $^5S_2$ (Ho^{3+}) are quite easy depopulated, and green emission is effectively quenched in the case of highly holmium-concentrated systems. These effects are due to cross-relaxation channels, i.e., the resonant cross relaxation processes ($^5S_2$ + $^5F_4$:$^5I_8$)$\rightarrow$($^5I_4$:$^5I_7$) and ($^5S_2$ + $^5F_4$:$^5I_8$)$\rightarrow$($^5I_7$:$^5I_4$) as well as the phonon-assisted cross-relaxation ($^5S_2$ + $^5F_4$:$^5I_8$)$\rightarrow$($^5I_6$:$^5I_7$). It was presented well and discussed earlier for $LiPbB_5O_9$:Ho^{3+} [51].

Additionally, the CIE chromaticity coordinates (x, y) for the studied LMG ceramic samples excited at 453 nm were calculated from the registered emission spectra in the visible range. The results are given in Table 1. It is clearly seen that the increasing concentrations of holmium ions in Li_2MgGeO_4 germanate ceramics caused changes in the x and y coordinates of the chromaticity parameters.

Table 1. The values of CIE chromaticity coordinates for LMG-Ho^{3+} ceramic systems.

Ceramic Code	CIE Coordinates	
	x	y
LMG-0.5Ho^{3+}	0.338	0.627
LMG-2.5Ho^{3+}	0.427	0.523
LMG-5.0Ho^{3+}	0.468	0.488

The chromaticity diagram shows the luminescence color modification from green through yellowish to nearly orange for ceramic systems doped with 0.5, 2.5, and 5 mol% Ho^{3+} concentrations, respectively. It is illustrated in Figure 5.

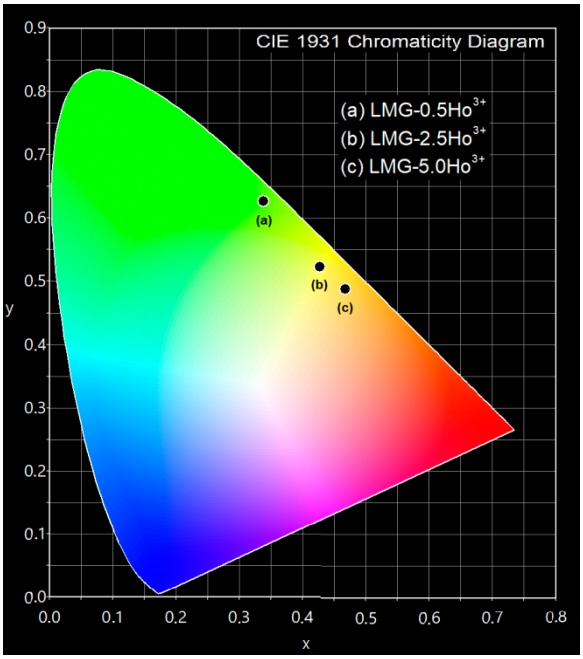

Figure 5. The influence of Ho^{3+} concentration on chromaticity coordinates for Li_2MgGeO_4 ceramics.

Luminescence decays from the excited states of holmium ions in Li_2MgGeO_4 ceramics were carried out to fully characterize the studied systems. It is clearly seen in Figure 6 that all registered decay profiles are nearly exponential, independent of the content of optically active dopants. Based on the decays, the luminescence lifetimes for the $^5F_4 + {}^5S_2$ (λ_{em} = 546 nm) and $^5F_5$ (λ_{em} = 666 nm) levels of Ho^{3+} were evaluated. The τ_m values for LMG-Ho^{3+} ceramics are nearly 10 µs ($^5F_4 + {}^5S_2$) and 6 µs ($^5F_5$). Moreover, it was observed that this spectroscopic parameter is practically independent of the concentration of Ho^{3+} ions in ceramic samples. The measured emission lifetimes for the $^5F_4 + {}^5S_2$ states of Ho^{3+} in the LMG host are similar to fluorophosphate glass [6], but they are relatively lower compared to other reported glasses [7], ceramics [52], and crystals [53].

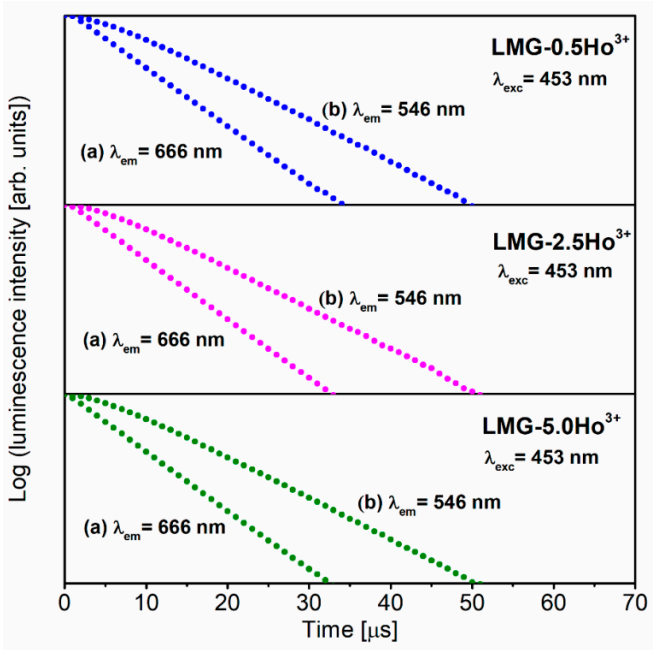

Figure 6. Decay curves for LMG-Ho^{3+} ceramics with different contents of holmium ions.

3.3. Luminescence Properties under Different Excitation Wavelengths

In order to study the luminescence properties of LMG-Ho^{3+} ceramics, the excitation spectra were registered at selected monitoring wavelengths. The results are presented in Figure 7. The excitation spectrum for LMG monitored at λ_{em} = 500 nm shows a broad band located at about 385 nm. Based on previous investigations, it was found that this phenomenon is related to the occurrence of magnesium in ceramics. It was proposed that the band in this spectral region is assigned to the excitation band of MgO [54–57]. On the other hand, the excitation spectrum for the LMG-Ho^{3+} ceramic monitored at the emission wavelength λ_{em} = 660 nm consists of several narrow and well-resolved bands. These bands were assigned to characteristic electronic transitions originating from the ground state, $^5I_8$, to the higher-lying states of trivalent Ho^{3+}. The following transitions of Ho^{3+} ions centered at about 453 nm, 485 nm, and 543 nm were identified as $^5I_8 \rightarrow {}^5G_6$, $^5I_8 \rightarrow {}^5F_{2,3}$, and $^5I_8 \rightarrow {}^5S_2, {}^5F_4$, respectively. Among the registered bands, the most intense band is located near 453 nm, corresponding to the $^5I_8 \rightarrow {}^5G_6$ (λ_{em} = 453 nm) transition of Ho^{3+}. Moreover, it was also observed in the 350–430 nm spectral region that bands assigned to the $^5I_8 \rightarrow {}^3H_{5,6}$ and $^5I_8 \rightarrow {}^5G_{4,5}$ transitions of Ho^{3+} overlapped with the excitation of the ceramic matrix. Therefore, it is possible to obtain the characteristic luminescence associated with trivalent Ho^{3+} ions by the direct excitation of the LMG host. This hypothesis was verified using the emission spectra measurements at selected excitation wavelengths. The ceramic samples were excited at the appropriate wavelengths assigned directly to the transitions of Ho^{3+} as well as the LMG ceramic matrix, and they are referred to by diamonds and asterisks in Figure 7.

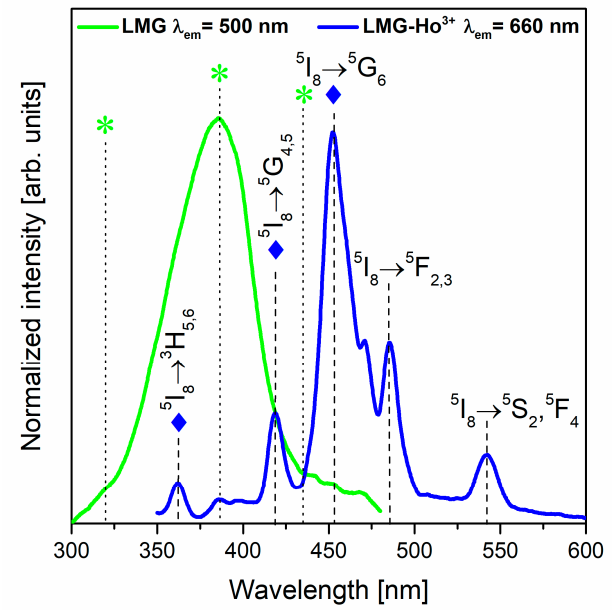

Figure 7. Excitation spectra of LMG and LMG-Ho^{3+} ceramics.

Figure 8 presents the emission spectra of LMG-0.5Ho^{3+} ceramics measured under the direct excitation of holmium ions (on the left) and the ceramic matrix (on the right). In the spectra, a broad luminescence band with a tail extending to about 700 nm could be distinguished as originating from the ceramic matrix. It is also worth emphasizing that the broad band from the LMG ceramic matrix overlapped with the narrow emission bands characteristic of Ho^{3+} ions. Depending on the excitation wavelengths, blue or greenish-blue broad emission was observed, similar to the excellent results obtained previously for MgO films, and these phenomena are related to the occurrence of defects and oxygen vacancies in MgO assigned to F-type centers [57]. After analyzing the literature data, it is suggested that the broad blue emission band is due to the presence of magnesium in the LMG ceramic matrix.

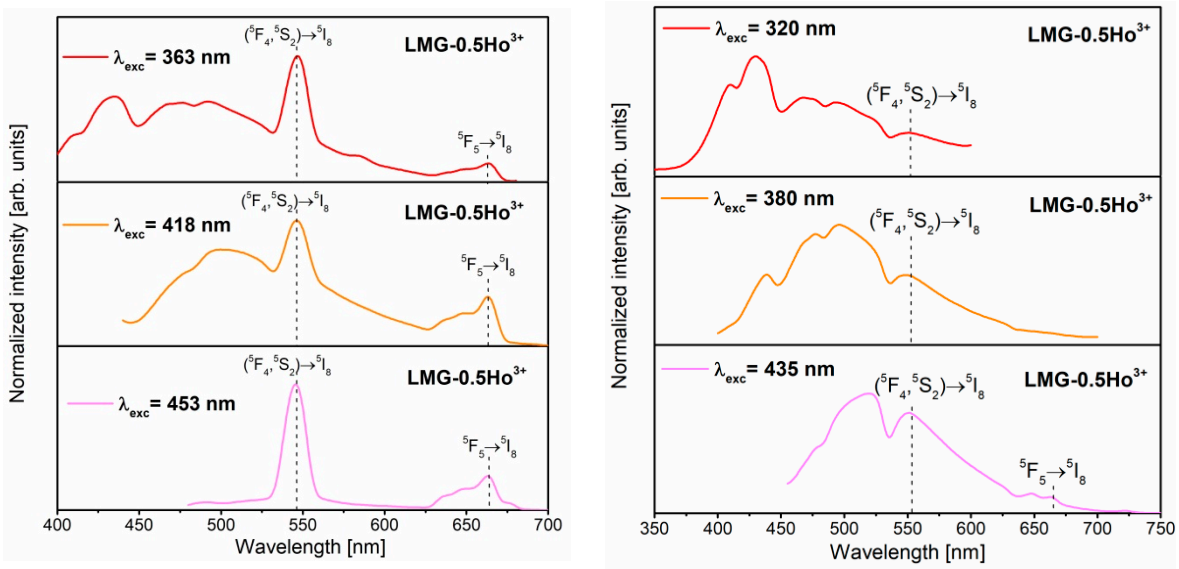

Figure 8. Emission spectra of LMG-Ho^{3+} under direct excitation of holmium ions (**left**) and host matrix (**right**).

The spectroscopic analysis indicates that the relative intensities of the emission bands attributed to the LMG host and Ho^{3+} ions are significantly dependent on the excitation wavelength. The green and red emission bands associated with $^5F_4,^5S_2 \rightarrow ^5I_8$ and $^5F_5 \rightarrow ^5I_8$ transitions are the most intense for ceramic samples during the direct excitation of Ho^{3+} ions. Additionally, the emission spectra of LMG-0.5Ho^{3+} samples excited at 363 nm and 418 nm contain broad blue band characteristic for the ceramic matrix. This is due to the fact that these excitation lines of Ho^{3+} overlap with the excitation spectrum of the matrix, as mentioned above. The characteristic band corresponding to the emission of the ceramic matrix becomes insignificant in the spectrum recorded upon the excitation by the 453 nm line.

Interesting results were obtained for LMG-0.5Ho^{3+} samples under the direct excitation of the ceramic matrix. The samples were excited at 320, 380, or 435 nm. The luminescence intensities of the broad band characteristic for the ceramic matrix were considerably higher in reference to the results obtained for the same LMG-0.5Ho^{3+} samples but measured under the direct excitation of holmium. Additionally, green emission bands at 550 nm, due to the $^5F_4,^5S_2 \rightarrow ^5I_8$ transitions of Ho^{3+}, are also well-observed during the excitation of the ceramic matrix. The presence of characteristic bands for trivalent holmium ions may indicate the energy transfer between the LMG ceramic matrix and the optical active dopants. Further investigations are in progress.

4. Conclusions

In this work, preliminary results for Li_2MgGeO_4:Ho^{3+} ceramics, referred to as LMG-Ho^{3+}, are presented and discussed. The X-ray diffraction analysis confirmed the presence of crystalline phase belonging to the monoclinic Li_2MgGeO_4. The luminescence spectra consisted of characteristic narrow bands in the green and red spectral regions, which correspond to the $^5F_4,^5S_2 \rightarrow ^5I_8$ and $^5F_5 \rightarrow ^5I_8$ transitions of Ho^{3+} ions. Their relative integrated emission intensities depend significantly on activator concentration. The emission intensity of the green band decreased rapidly, whereas the intensity of the red emission was enhanced by increasing Ho^{3+} concentrations. In particular, the emission spectra of Li_2MgGeO_4:Ho^{3+} were examined under different excitation wavelengths. The emission spectra were measured under the direct excitation of Ho^{3+} ions and the ceramic matrix. The spectroscopic analysis revealed the presence of broad blue luminescence, which was assigned to the ceramic matrix, and narrow emission bands characteristic of the 4f-4f transi-

tions of Ho^{3+}. Further studies suggest an energy transfer between the LMG ceramic matrix and the Ho^{3+} ions.

Author Contributions: Conceptualization, J.P.; methodology, M.K., E.P., T.G. and B.M.; software, N.B.-A.; formal analysis, W.A.P.; investigation, N.B.-A., M.K., E.P., W.A.P., T.G., B.M. and J.P.; writing—original draft preparation, N.B.-A. and J.P.; writing—review and editing, J.P.; visualization, N.B.-A.; supervision, W.A.P.; project administration, J.P.; funding acquisition, J.P. All authors have read and agreed to the published version of the manuscript.

Funding: This research was funded by the National Science Centre (Poland), grant number 2019/35/B/ST5/01924.

Institutional Review Board Statement: Not applicable.

Informed Consent Statement: Not applicable.

Data Availability Statement: Not applicable.

Conflicts of Interest: The authors declare no conflict of interest.

References

1. Lim, C.S.; Aleksandrovsky, A.; Molokeev, M.; Oreshonkov, A.; Atuchin, V. The modulated structure and frequency upconversion properties of $CaLa_2(MoO_4)_4$:Ho^{3+}/Yb^{3+} phosphors prepared by microwave synthesis. *Phys. Chem. Chem. Phys.* **2015**, *17*, 19278–19287. [CrossRef] [PubMed]
2. Sukhachev, A.L.; Malakhovskii, A.V.; Aleksandrovsky, A.S.; Gudim, I.A.; Temerov, V.L. Spectroscopic properties of $HoFe_3(BO_3)_4$, $NdFe_3(BO_3)_4$ and $Ho_{0.75}Nd_{0.25}Fe_3(BO_3)_4$ single crystals. *Opt. Mater.* **2018**, *83*, 87–92. [CrossRef]
3. Denisenko, Y.G.; Atuchin, V.V.; Molokeev, M.S.; Wang, N.; Jiang, X.; Aleksandrovsky, A.S.; Krylov, A.S.; Oreshonkov, A.S.; Sedykh, A.E.; Volkova, S.S.; et al. Negative thermal expansion in one-dimension of a new double sulfate $AgHo(SO_4)_2$ with isolated SO_4 tetrahedra. *J. Mater. Sci. Technol.* **2021**, *76*, 111–121. [CrossRef]
4. Lim, C.-S.; Aleksandrovsky, A.; Molokeev, M.; Oreshonkov, A.; Atuchin, V. Structural and Spectroscopic Effects of Li^+ Substitution for Na^+ in $Li_xNa_{1-x}CaGd_{0.5}Ho_{0.05}Yb_{0.45}(MoO_4)_3$ Scheelite-Type Upconversion Phosphors. *Molecules* **2021**, *26*, 7357. [CrossRef]
5. Srinivasa Rao, C.; Upendra Kumar, K.; Babu, P.; Jayasankar, C.K. Optical properties of Ho^{3+} ions in lead phosphate glasses. *Opt. Mater.* **2012**, *35*, 102–107. [CrossRef]
6. Jayachandra Prasad, T.; Neelima, G.; Ravi, N.; Kiran, N.; Nallabala, N.K.R.; Kummara, V.K.; Suresh, K.; Gadige, P. Optical and spectroscopic properties of Ho^{3+}-doped fluorophosphate glasses for visible lighting applications. *Mater. Res. Bull.* **2020**, *124*, 110753. [CrossRef]
7. Ravi Prakash, M.; Neelima, G.; Kummara, V.K.; Ravic, N.; Dwaraka Viswanath, C.S.; Subba Rao, T.; Mahaboob Jilani, S. Holmium doped bismuth-germanate glasses for green lighting applications: A spectroscopic study. *Opt. Mater.* **2019**, *94*, 436–443. [CrossRef]
8. Pisarska, J.; Kuwik, M.; Górny, A.; Kochanowicz, M.; Zmojda, J.; Dorosz, J.; Dorosz, D.; Sitarz, M.; Pisarski, W.A. Holmium doped barium gallo-germanate glasses for near-infrared luminescence at 2000 nm. *J. Lumin.* **2019**, *215*, 116625. [CrossRef]
9. Devaraja, C.; Jagadeesha Gowda, G.V.; Eraiah, B.; Keshavamurthy, K. Optical properties of bismuth tellurite glasses doped with holmium oxide. *Ceram. Int.* **2021**, *47*, 7602–7607. [CrossRef]
10. Lu, D.-Y.; Guan, D.-X. Photoluminescence associated with the site occupations of Ho^{3+} ions in $BaTiO_3$. *Sci. Rep.* **2017**, *7*, 6125. [CrossRef]
11. Lu, B.; Cheng, H.; Xu, X.; Chen, H. Preparation and characterization of transparent magneto-optical Ho_2O_3 ceramics. *J. Am. Ceram. Soc.* **2019**, *102*, 118–122. [CrossRef]
12. Pan, Y.; Bai, X.; Feng, J.; Huang, L.; Li, G.; Chen, Y. Influences of holmium substitution on the phase structure and piezoelectric properties of $BiFeO_3$-$BaTiO_3$-based ceramics. *J. Alloys Compd.* **2022**, *918*, 165582. [CrossRef]
13. Tsotetsi, D.; Dhlamini, M.; Mbule, P. Sol-gel synthesis and characterization of Ho^{3+} doped TiO_2 nanoparticles: Evaluation of absorption efficiency and electrical conductivity for possible application in perovskite solar cells. *Opt. Mater.* **2022**, *130*, 112569. [CrossRef]
14. Wu, X.; Lin, J.; Chen, P.; Liu, C.; Lin, M.; Cong Lin, C.; Luo, L.; Zheng, X. Ho^{3+}-doped (K,Na)NbO_3-based multifunctional transparent ceramics with superior optical temperature sensing performance. *J. Am. Ceram. Soc.* **2019**, *102*, 1249–1258. [CrossRef]
15. Lin, J.; Lu, Q.; Xu, K.; Wu, X.; Lin, C.; Lin, T.; Chen, C.; Luo, L. Outstanding optical temperature sensitivity and dual-mode temperature-dependent photoluminescence in Ho^{3+}-doped (K,Na)NbO_3-$SrTiO_3$ transparent ceramics. *J. Am. Chem. Soc.* **2019**, *102*, 4710–4720. [CrossRef]
16. Li, J.; Chai, X.; Wang, X.; Xu, C.-N.; Gu, Y.; Zhao, H.; Yao, X. Large electrostrain and high optical temperature sensitivity in $BaTiO_3$-$(Na_{0.5}Ho_{0.5})TiO_3$ multifunctional ferroelectric ceramics. *Dalton Trans.* **2016**, *45*, 11733–11741. [CrossRef]
17. Yun, X.; Zhou, J.; Zhu, Y.; Li, X.; Xu, D. Up-conversion luminescence and optical temperature sensing properties of Ho^{3+}-doped double-tungstate $LiYb(WO_4)_2$ phosphors. *J. Mater. Sci. Mater. Electron.* **2021**, *32*, 17990–18001. [CrossRef]

18. Wu, J.; Ma, C.; Fan, Y.; Sun, B.; Sheng, Y.; Zhai, Z.; Lu, H.; Lv, X. Upconversion luminescence and non-contact optical temperature sensing in Ho^{3+}-doped $0.94Na_{0.5}Bi_{0.5}TiO_3$-$0.06BaTiO_3$ lead-free ceramics. *Opt. Mater.* **2022**, *127*, 112239. [CrossRef]
19. Zhao, Y.; Wang, X.; Zhang, Y.; Li, Y.; Yao, X. Optical temperature sensing of up-conversion luminescent materials: Fundamentals and progress. *J. Alloys Compd.* **2020**, *817*, 152691. [CrossRef]
20. Ye, Y.; Tang, Z.; Ji, Z.; Xiao, H.; Liu, Y.; Qin, Y.; Liang, L.; Qi, J.; Lu, T. Fabrication and luminescent properties of holmium doped $Y_2Zr_2O_7$ transparent ceramics as new type laser material. *Opt. Mater.* **2021**, *121*, 111643. [CrossRef]
21. Safronova, N.A.; Yavetskiy, R.P.; Kryzhanovska, O.S.; Dobrotvorska, M.V.; Balabanov, A.E.; Vorona, I.O.; Tolmachev, A.V.; Baumer, V.N.; Matolínova, I.; Kosyanov, D.Y.; et al. A novel IR-transparent Ho^{3+}:Y_2O_3–MgO nanocomposite ceramics for potential laser applications. *Ceram. Int.* **2021**, *47*, 1399–1406. [CrossRef]
22. Jin, Y.; Hu, Y.; Chen, L.; Ju, G.; Wu, H.; Mu, Z.; He, M.; Xue, F. Luminescent properties of a green long persistent phosphor Li_2MgGeO_4:Mn^{2+}. *Opt. Mater. Exp.* **2016**, *6*, 929–937. [CrossRef]
23. Zhu, Y.-F.; Jiang, T.; Li, L.; Cheng, L.-X.; Zhang, J.-C. Short-Term Non-Decaying Mechanoluminescence in Li_2MgGeO_4:Mn^{2+}. *Materials* **2020**, *13*, 1410. [CrossRef]
24. Bai, Y.; Zheng, Z.; Wu, L.; Kong, Y.; Zhang, Y.; Xu, J. Construction of a novel mechanoluminescent phosphor Li_2MgGeO_4:xMn^{2+} by defect control. *Dalton Trans.* **2021**, *50*, 8803–8810. [CrossRef]
25. Huang, S.; Li, G. Photoluminescence properties of Li_2SrGeO_4:RE^{3+} (RE = Ce/Tb/Dy) phosphors and enhanced luminescence through energy transfer between Ce^{3+} and Tb^{3+}/Dy^{3+}. *Opt. Mater.* **2014**, *36*, 1555–1560. [CrossRef]
26. Fang, W.; Ao, L.; Tang, Y.; Li, J.; Xiang, H.; Zhang, Z.; Du, Q.; Fang, L. Phase evolution and microwave dielectric properties of the $Li_{2(1+x)}ZnGe_3O_8$ spinel oxides. *J. Mater. Sci. Mater. Electron.* **2020**, *31*, 13496–13502. [CrossRef]
27. Li, C.; Yin, C.; Chen, J.; Xiang, H.; Tang, Y.; Fang, L. Crystal structure and dielectric properties of germanate melilites $Ba_2MGe_2O_7$ (M = Mg and Zn) with low permittivity. *J. Eur. Ceram. Soc.* **2018**, *38*, 5246–5251. [CrossRef]
28. Chen, C.X.; Wu, S.P.; Fan, Y.X. Synthesis and microwave dielectric properties of B_2O_3-doped Mg_2GeO_4 ceramics. *J. Alloys Compd.* **2013**, *578*, 153–156. [CrossRef]
29. Yang, Z.; Tang, Y.; Li, J.; Fang, W.; Ma, J.; Yang, A.; Liu, L.; Fang, L. Crystal structure, Raman spectra and microwave dielectric properties of novel low-temperature cofired ceramic Li_4GeO_4. *J. Alloys Compd.* **2021**, *867*, 159059. [CrossRef]
30. Koseva, I.; Nikolov, V.; Petrova, N.; Tzvetkov, P.; Marychev, M. Thermal behavior of germanates with olivine structure. *Thermochim. Acta* **2016**, *646*, 1–7. [CrossRef]
31. Zhou, S.; Wang, X.; He, S.; Chen, X.; Wu, Y.; Zhou, H. Microstructural evolution, dielectric performance, and densification behavior of novel $NaAGeO_4$ (A = Sm, Y) ceramics. *Ceram. Int.* **2022**, *48*, 16386–16390. [CrossRef]
32. Li, C.; Xiang, H.; Xu, M.; Tang, Y.; Fang, L. Li_2AGeO_4 (A = Zn, Mg): Two novel low-permittivity microwave dielectric ceramics with olivine structure. *J. Eur. Ceram. Soc.* **2018**, *38*, 1524–1528. [CrossRef]
33. Shang, M.; Li, G.; Yang, D.; Kang, X.; Peng, C.; Lin, J. Luminescence properties of Mn^{2+}-doped Li_2ZnGeO_4 as an efficient green phosphor for field-emission displays with high color purity. *Dalton Trans.* **2012**, *41*, 8861–8868. [CrossRef] [PubMed]
34. Fu, Y.; Zhang, S.; Hu, Y. Enhanced red-emitting phosphor $Na_2Ca_3Si_2O_8$:Eu^{3+} by charge compensation. *J. Mater. Sci. Mater. Electron.* **2017**, *28*, 5262–5269. [CrossRef]
35. Puchalska, M.; Watras, A. A clear effect of charge compensation through Na^+ co-doping on luminescent properties of new $CaGa_4O_7$:Nd^{3+}. *J. Alloys Compd.* **2016**, *688*, 253–260. [CrossRef]
36. Puchalska, M.; Zych, E. The effect of charge compensation by means of Na^+ ions on the luminescence behavior of Sm^{3+}-doped $CaAl_4O_7$ phosphor. *J. Lumin.* **2012**, *132*, 826–831. [CrossRef]
37. Nagabhushana, H.; Sunitha, D.V.; Sharma, S.C.; Daruka Prasad, B.; Nagabhushana, B.M.; Chakradhar, R.P.S. Enhanced luminescence by monovalent alkali metal ions in Sr_2SiO_4:Eu^{3+} nanophosphor prepared by low temperature solution combustion method. *J. Alloys Compd.* **2014**, *595*, 192–199. [CrossRef]
38. Tang, W.; Guo, Q.; Su, K.; Liu, H.; Zhang, Y.; Mei, L.; Liao, L. Structure and photoluminescence properties of Dy^{3+} doped phosphor with whitlockite structure. *Materials* **2022**, *15*, 2177. [CrossRef]
39. Praveena, R.; Sravani Sameera, V.; Babu, P.; Basavapoornima, C.; Jayasankar, C.K. Photoluminescence properties of Ho^{3+}/Tm^{3+}-doped YAGG nanocrystalline powders. *Opt. Mater.* **2017**, *72*, 666–672. [CrossRef]
40. Atuchin, V.V.; Aleksandrovsky, A.S.; Chimitova, O.D.; Krylov, A.S.; Molokeev, M.S.; Bazarov, B.G.; Bazarova, J.G.; Xia, Z. Synthesis and spectroscopic properties of multiferroic β′-$Tb_2(MoO_4)_3$. *Opt. Mater.* **2014**, *36*, 1631–1635. [CrossRef]
41. Atuchin, V.V.; Aleksandrovsky, A.S.; Chimitova, O.D.; Diao, C.-P.; Gavrilova, T.A.; Kesler, V.G.; Molokeev, M.S.; Krylov, A.S.; Bazarov, B.G.; Bazarova, J.G.; et al. Electronic structure of β-$RbSm(MoO_4)_2$ and chemical bonding in molybdates. *Dalton Trans.* **2015**, *44*, 1805–1815. [CrossRef]
42. Denisenko, Y.G.; Atuchin, V.V.; Molokeev, M.S.; Sedykh, A.E.; Khritokhin, N.A.; Aleksandrovsky, A.S.; Oreshonkov, A.S.; Shestakov, N.P.; Adichtchev, S.V.; Pugachev, A.M.; et al. Exploration of the Crystal Structure and Thermal and Spectroscopic Properties of Monoclinic Praseodymium Sulfate $Pr_2(SO_4)_3$. *Molecules* **2022**, *27*, 3966. [CrossRef]
43. Tran, L.T.N.; Massella, D.; Zur, L.; Chiasera, A.; Varas, S.; Armellini, C.; Righini, G.C.; Lukowiak, A.; Zonta, D.; Ferrari, M. SiO_2-SnO_2:Er^{3+} Glass-Ceramic Monoliths. *Appl. Sci.* **2018**, *8*, 1335. [CrossRef]
44. Fernández-Rodríguez, L.; Balda, R.; Fernández, J.; Durán, A.; Pascual, M.J. Role of Eu^{2+} and Dy^{3+} Concentration in the Persistent Luminescence of $Sr_2MgSi_2O_7$ Glass-Ceramics. *Materials* **2022**, *15*, 3068. [CrossRef]

45. Pawlik, N.; Szpikowska-Sroka, B.; Goryczka, T.; Pisarska, J.; Pisarski, W.A. Structural and Photoluminescence Investigations of Tb^{3+}/Eu^{3+} Co-Doped Silicate Sol-Gel Glass-Ceramics Containing CaF_2 Nanocrystals. *Materials* **2021**, *14*, 754. [CrossRef]
46. Pirri, A.; Maksimov, R.N.; Li, J.; Vannini, M.; Toci, G. Achievements and Future Perspectives of Trivalent Thulium-Ion-Doped Mixed Sesquioxide Ceramics for Laser Applications. *Materials* **2022**, *15*, 2084. [CrossRef]
47. Miniajluk-Gaweł, N.; Bondzior, B.; Lemanski, K.; Vu, T.H.Q.; Stefańska, D.; Boulesteix, R.; Dereń, P.J. Effect of Ceramic Formation on the Emission of Eu^{3+} and Nd^{3+} Ions in Double Perovskites. *Materials* **2021**, *14*, 5996. [CrossRef]
48. Siva Sesha Reddy, A.; Purnachand, N.; Kostrzewa, M.; Brik, M.G.; Venkatramaiah, N.; Ravi Kumar, V.; Veeraiah, N. The role of gold metallix particles on improving green and NIR emissions of Ho^{3+} ions in non-conventional SeO_2 based glass ceramics. *J. Non-Cryst. Solid* **2022**, *576*, 121240. [CrossRef]
49. Singh, V.; Lakshminarayana, G.; Wagh, A.; Singh, N. Luminescence features of green-emitting $CaLa_4Si_3O_{13}:Ho^{3+}$ phosphors. *Optik* **2020**, *207*, 164284. [CrossRef]
50. Li, W.; Hao, J.; Fu, P.; Du, J.; Li, P.; Li, H.; Li, W.; Yue, Z. High-temperature and long-term stability of Ho-doped potassium sodium niobate-based multifunctional ceramics. *Ceram. Int.* **2021**, *47*, 13391–13401. [CrossRef]
51. Raman, T.R.; Vijayalakshmi, R.P.; Ratnakaram, Y.C. Effect of Ho^{3+} ion concentration on structure and spectroscopic properties of $LiPbB_5O_9:Ho^{3+}$ phosphor. *J. Mol. Struct.* **2021**, *1243*, 130759. [CrossRef]
52. Georgescu, S.; Stefan, A.; Toma, O.; Voiculescu, A.-M. Judd-Ofelt analysis of Ho^{3+} doped in ceramic $CaSc_2O_4$. *J. Lumin.* **2015**, *162*, 174–179. [CrossRef]
53. Kaczkan, M.; Malinowski, M. Optical Transitions and Excited State Absorption Cross Sections of $SrLaGaO_4$ Doped with Ho^{3+} Ions. *Materials* **2021**, *14*, 3831. [CrossRef]
54. Zhang, J.; Zhang, L. Intensive green light emission from MgO nanobelts. *J. Phys. Chem. Lett.* **2002**, *363*, 293–297. [CrossRef]
55. Janet, C.M.; Viswanathan, B.; Viswanath, R.P.; Varadarajan, T.K. Characterization and photoluminescence properties of MgO microtubes synthesized from hydromagnesite flowers. *J. Phys. Chem. C* **2007**, *111*, 10267–10272. [CrossRef]
56. Uchino, T.; Okutsu, D. Broadband laser emission from color centers inside MgO microcrystals. *Phys. Rev. Lett.* **2008**, *101*, 117401. [CrossRef] [PubMed]
57. Martinez-Boubeta, C.; Martinez, A.; Hernandez, S.; Pellegrino, P.; Antony, A.; Bertomeu, J.; Balcells, L.; Konstantinovic, Z.; Martinez, B. Blue luminescence at room temperature in defective MgO films. *Solid State Commun.* **2011**, *151*, 751–753. [CrossRef]